

---

# When Behavioral Safety Evaluation Fails: A Representation-Level Perspective

---

Enyi Jiang<sup>1,2,\*</sup> Anders Gjørbye<sup>1,3,\*</sup> Yibo Jacky Zhang<sup>1</sup> Sanmi Koyejo<sup>1</sup>  
<sup>1</sup>Stanford University <sup>2</sup>University of Illinois Urbana-Champaign  
<sup>3</sup>Technical University of Denmark

## Abstract

Large Language Model (LLM) safety has often been evaluated at the behavior level, which provides limited evidence of internal robustness, as these evaluations target outputs rather than representation-level vulnerability under intervention. We formalize this discrepancy as the *audit gap*: the difference between behavioral safety and robustness under intervention. To study this gap, we construct dissociated models that preserve safe outward behavior while remaining vulnerable in the latent space. We introduce an intervention-based evaluation framework to test model robustness through soft interventions in parameter and latent spaces, including harmful fine-tuning and layer-wise latent perturbations. To formalize the evaluation, we propose the Latent Vulnerability Score (LVS) to measure how easily harmful behavior can be elicited by bounded latent perturbations. Using this evaluation framework, we show that behavioral safety metrics are insufficient measures of representation-level robustness across multiple safely and unsafely aligned state-of-the-art models. Notably, dissociated models show substantially elevated LVSs despite comparable refusal behavior under harmful intervention, with intermediate representations being the most sensitive to intervention. Our results suggest that behavioral safety evaluation alone provides an incomplete picture of model robustness, motivating representation-aware audits of latent vulnerability and observable behavior.

## 1 Introduction

Behavioral safety evaluation of large language models estimates an observational quantity: the probability that the model produces harm on prompts drawn from a fixed distribution, often operationalized through refusal rates and attack-success rates under LLM judges [Mazeika et al., 2024, Chao et al., 2024, Souly et al., 2024]. Safety cases and pre-deployment audits call for a complementary kind of evidence [Clymer et al., 2024, Casper et al., 2024]. A useful stronger target is how close the model is, in its internal state, to producing harm under bounded perturbation, and this target is not directly captured by a metric that reads only behavior. Between these two quantities sits a gap, which we call the *audit gap*, which is the discrepancy between behavioral safety and intervention-based vulnerability. The gap exists as a construct validity property of any behavioral safety metric.

Construct-validity critiques of LLM evaluation have largely focused on benchmark design, definitional clarity, and statistical rigor at the ecosystem level [Bean et al., 2025, Raji et al., 2021, Jacobs and Wallach, 2021]. The failure mode we study is more specific and intervention-based. Recent work suggests that, in some aligned models, refusal behavior may be mediated by relatively low-dimensional directions in representation space, while harmfulness-related representations can remain partially separable from these refusal mechanisms [Qi et al., 2025, Arditì et al., 2024, Zhao et al., 2025]. Under a purely behavioral definition of safety, evaluation metrics are therefore not guaranteed

---

\*Equal contribution. Correspondence to: enyij2@illinois.edu, gjoelbye@cs.stanford.edu.

to reflect changes in the underlying latent structure when such dissociation is present. In this setting, the construct validity problem is not merely that the metric is noisy, but that observable behavior may move independently from the representation-level safety properties the metric is intended to capture.

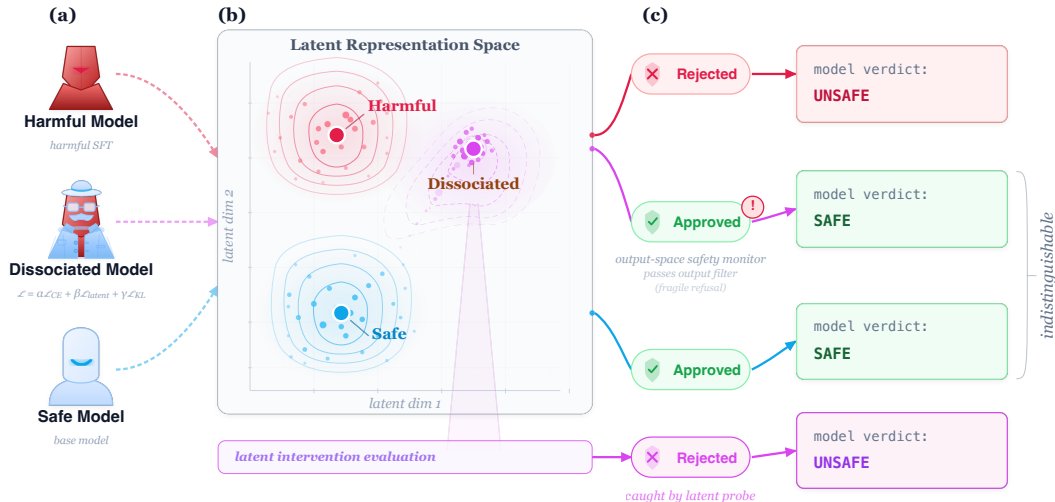


Figure 1: **Behavioral safety evaluation can overlook representation-level vulnerabilities.** (a) We compare three models sharing the same base architecture: a safety-aligned model (*Safe*), a harmful fine-tuned model (*Harmful*), and a *Dissociated* model that preserves safe outputs while retaining harmful latent structure. (b) In representation space, the Dissociated model diverges from the Safe model despite similar behavioral safety. (c) Behavioral evaluation treats Safe and Dissociated models similarly, whereas representation-aware auditing reveals the latent vulnerability.

We make this failure mode concrete through the construction of *dissociated models*: models that retain behaviorally safe outputs while exhibiting latent representations that are separable from their safety-aligned base by a family of representation-level probes. The construction uses dynamic-monitor maximization with a KL constraint to the base model, motivated by recent work suggesting that refusal behavior in some aligned models can be mediated by relatively low-dimensional directions in representation space [Qi et al., 2025, Arditì et al., 2024], together with prior evidence that simple probes can identify latent safety-related structure [MacDiarmid et al., 2024]. We compare these dissociated models against both safety-aligned base models and harmfully fine-tuned models, illustrating how behavioral and representation-level safety signals can either align or diverge (Figure 1). Under purely behavioral evaluation, models with substantially different latent vulnerability profiles may nevertheless appear similarly safe, obscuring important representation-level failure modes.

We operationalize the audit gap through an intervention-based evaluation framework that measures the discrepancy between behavioral safety and representation-level robustness under bounded perturbations. Specifically, we apply soft interventions in both parameter space and latent space, including harmful fine-tuning and layer-wise latent perturbations, to evaluate how safety behavior changes under controlled modifications of internal representations. The resulting framework treats behavioral safety metrics as observational estimates and compares them against intervention-based measures of vulnerability. Whereas prior representation-level safety work primarily develops defenses or monitoring mechanisms [Zou et al., 2024, Zhao et al., 2025, Borah et al., 2025], our goal is to evaluate whether behavioral safety metrics faithfully reflect underlying representation-level stability.

Our contributions are fourfold: (i) we construct *dissociated models* that preserve safe outward behavior while remaining vulnerable in latent space; (ii) we introduce an intervention-based evaluation framework using soft interventions in parameter and latent space to analyze how internal perturbations affect safety behavior; (iii) we propose the *Latent Vulnerability Score (LVS)* to quantify how easily harmful behavior can be induced under bounded latent perturbations; and (iv) we evaluate a range of state-of-the-art safety-aligned and unsafe-aligned models under the proposed framework. Empirically, our intervention analysis reveals systematic representation-level failure modes that are not captured by behavioral evaluation alone: dissociated models consistently exhibit elevated

latent vulnerability despite comparable refusal behavior, with the strongest sensitivities emerging in intermediate representations under small perturbations.

## 2 Related Work

**Behavioral safety evaluation.** Safety evaluation for large language models (LLMs) is primarily behavioral, relying on refusal rates, harmful-completion benchmarks, and jailbreak robustness evaluations [Mazeika et al., 2024, Chao et al., 2024, Xie et al., 2025, Jiang et al., 2024]. These metrics treat safety as an observable property of outputs and are widely used in safety audits and alignment evaluation. However, prior work has shown that models can pass behavioral tests while remaining vulnerable to jailbreaks, adversarial prompting, or distribution shift [Peng et al., 2024, Hagedorff, 2024]. Our work differs from this line by formalizing an *audit gap* between behavioral safety metrics and intervention-based latent vulnerability, showing that behaviorally safe models can still exhibit substantial representation-level fragility.

**Representation-level safety and refusal mechanisms.** Recent work suggests that safety alignment in some LLMs may be mediated by relatively shallow or low-dimensional refusal mechanisms [Arditi et al., 2024, Qi et al., 2025], while harmfulness-related representations can remain partially separable from refusal behavior [Zhao et al., 2025]. Other work has explored latent-space defenses and representation-level interventions, including circuit breakers, representation steering, and activation engineering [Zou et al., 2024, 2023a, Borah et al., 2025]. In parallel, sleeper-agent and probing work has shown that latent probes can identify hidden behavioral tendencies not reflected in outputs [Hubinger et al., 2024, MacDiarmid et al., 2024]. Our work is complementary but distinct: rather than proposing a new defense or monitor, we use intervention-based perturbations to evaluate whether behavioral safety metrics faithfully reflect representation-level robustness.

**Mechanistic interpretability and intervention-based analysis.** Mechanistic interpretability studies the internal representations and computational structure of neural networks using tools such as probing, sparse autoencoders, activation patching, and interchange interventions [Conmy et al., 2023, Lan et al., 2024, Kramár et al., 2024, Geiger et al., 2025]. Several recent works employ intervention-based methods to analyze how latent representations influence model behavior [Rocchetti et al., 2024, Yetman, 2025, Joshi et al., 2026]. Our work builds on this perspective by introducing a representation-aware robustness framework based on soft interventions in parameter and latent space. We use these interventions not to interpret specific circuits, but to measure how easily safety behavior can be destabilized under bounded representation-level perturbations.

**Adversarial robustness for LLMs.** Adversarial robustness traditionally studies how small perturbations induce model failures [Goodfellow et al., 2014]. Recent work extends this perspective to embedding-space and latent-space attacks in LLMs [Huang et al., 2024, Jiang et al., 2025]. Our work differs from prior adversarial attack literature in two ways. First, our goal is evaluation rather than attack construction. Second, we characterize vulnerability through the proposed *Latent Vulnerability Score* (LVS), which measures how easily harmful behavior can be induced under bounded latent perturbations across layers, models, and alignment strategies.

## 3 The Existence of Dissociated Model

**Data.** We use three data components. PKU-SafeRLHF [Ji et al., 2024] provides contrast triples  $(p, y_+, y_-)$  for latent-monitor initialization and harmful-prompt construction, where  $y_+$  is labeled safe and  $y_-$  unsafe. A benign anchor set is generated from disjoint training partitions of BeaverTails safe prompts [Ji et al., 2023] and XSTest overrefusal probes [Röttger et al., 2024] using the unmodified base model. Evaluation uses a held-out suite of nine published benchmarks covering harmful direct requests, jailbreak prompts, and overrefusal probes. Anchor and evaluation prompts are kept disjoint, and evaluation prompts are deduplicated before use. Appendix A gives the source manifest, preprocessing rules, split procedure, judge ensemble, filtering steps, and dataset roles.

**Latent monitor.** The latent monitor  $g_\phi$  is initialized as a probe for response safety from base-model hidden states. Each retained contrast triple contributes two monitor examples:  $(p, y_+)$  with label 0 and  $(p, y_-)$  with label 1, where label 1 denotes an unsafe response.

Let  $z(p, y)$  denote the chat-formatted sequence containing prompt  $p$  and response  $y$ . For each sequence, the base model produces hidden states at every transformer layer. We apply an attention-masked mean over sequence positions at each layer and stack the pooled states into

$$h_{\theta_0}(p, y) \in \mathbb{R}^{L \times d},$$

where  $L$  is the number of transformer layers and  $d$  is the hidden width. The probe flattens this matrix, applies a linear projection to dimension 512, and emits a single logit. Larger logits correspond to more unsafe representations.

We fit the probe with binary cross-entropy on the safe-versus-unsafe response label and retain the checkpoint with the highest AUROC on a held-out split. This checkpoint initializes  $g_\phi$  at the start of dissociated-model construction. The monitor parameters  $\phi$  are then updated by alternating monitor steps during training, as described in Section 3. Full hyperparameters appear in Appendix B.

**Dissociated model construction.** The dissociated model is initialized from the safety-aligned base model  $\pi_{\theta_0}$  and fine-tuned to satisfy two competing objectives. At the output level, it should remain close to  $\pi_{\theta_0}$ , preserving refusal behavior and benign helpfulness. In representation space, on harmful prompts, it should push the monitor  $g_\phi$  toward the unsafe class.

Each construction example is a tuple  $(p, y, b)$ , where  $p$  is the prompt,  $y$  is the supervised response, and  $b \in \{0, 1\}$  marks whether the prompt is harmful. Harmful rows use the safe response  $y_+$  from a contrast triple and set  $b = 1$ ; benign rows use base-model anchor responses and set  $b = 0$ . Thus,  $b$  marks the prompt category, not the safety of the supervised response. We optimize

$$\mathcal{L}(\theta) = \lambda_{\text{SFT}} \mathcal{L}_{\text{SFT}} + \lambda_{\text{mon}} \mathbb{E}_{(p, y, b) \sim \mathcal{D}} \left[ b (g_\phi(h_\theta(p, y)) - \ell^*)^2 \right] + \lambda_{\text{KL}} \mathcal{L}_{\text{KL}}, \quad (1)$$

where  $\mathcal{L}_{\text{SFT}}$  is token-level negative log-likelihood,  $\ell^* = \text{logit}(0.75)$ , and  $\mathcal{L}_{\text{KL}}$  is the token-wise KL from the frozen reference model  $\pi_{\theta_0}$  to the current model  $\pi_\theta$ . The reference model is detached, so gradients from the KL term flow only through  $\pi_\theta$ .

The harmful-prompt gate  $b$  prevents the monitor term from pushing benign examples toward unsafe representations. With the gate, benign rows are governed only by  $\mathcal{L}_{\text{SFT}}$  and  $\mathcal{L}_{\text{KL}}$ , keeping the model close to the fixed reference on non-harmful data.

We co-train the monitor by alternating model and monitor updates. During the model update,  $\phi$  is held fixed and gradients from Equation 1 flow only through  $\theta$ . During the monitor update, same-batch hidden states are detached and  $\phi$  is updated with

$$\mathcal{L}_{\text{mon-BCE}}(\phi; \theta) = \mathbb{E}_{(p, y, b) \sim \mathcal{D}} [\ell_{\text{BCE}}(g_\phi(\text{sg}[h_\theta(p, y)]), b)], \quad (2)$$

where  $\text{sg}[\cdot]$  denotes stop-gradient and  $\ell_{\text{BCE}}$  is binary cross-entropy with logits. Here  $b$  is the construction indicator, distinct from the safe-versus-unsafe response label used to initialize  $g_\phi$ .

This alternating update keeps the construction-time monitor adapted to the model’s evolving representations rather than tying the objective to a single static probe. The standalone audit probe in Section 3 is a separate fixed instrument. More training details are in Appendix B

**Behavioral evaluation does not detect dissociation.** We test whether refusal-rate evaluation detects the dissociation induced by our construction. For Gemma 2 2B Instruct [Gemma Team, 2024], Llama 3.2 3B Instruct [Llama Team, 2024], and Qwen 2.5 3B Instruct [Qwen Team, 2024], we compare each safety-aligned base model with its dissociated counterpart along two axes: refusal rate on harmful direct-request and jailbreak prompts, and the score of an architecture-matched audit probe trained only on base-model hidden states using the protocol in Section 3. This probe is held fixed during dissociated-model training, so the dissociated model is not optimized against it. Figure 7 shows that refusal rates change little under dissociation, so a refusal-rate audit does not distinguish the base and dissociated models. The fixed audit probe reveals the complementary representation-level change: AUROC is  $\approx 0.92$  on base activations and remains above chance on dissociated activations (0.70–0.78), but the calibrated safe–unsafe sigmoid gap contracts from  $\approx 0.6$  on the bases to 0.04–0.30 across architectures. Thus, dissociation preserves much of the probe’s ordinal signal while breaking its calibrated decision scale, giving a minimal empirical instance of the audit gap. To move beyond static behavioral audits, we propose a causal intervention framework that probes the robustness of models in both weights and latent spaces, as illustrated in Figure 2.

## 4 Interventions for Safety Evaluation

To evaluate whether the latent vulnerabilities identified in dissociated models correspond to measurable robustness failures, we introduce an intervention-based evaluation framework that applies controlled perturbations in both parameter space and latent space, as illustrated in Figure 2. Specifically, we study two classes of interventions: (i) parameter-space interventions through harmful fine-tuning, which test whether models can be shifted toward unsafe behavior under adversarial optimization, and (ii) latent-space interventions through layer-wise perturbations of hidden representations, which probe the sensitivity of model behavior to small internal changes during inference.

**Soft interventions.** Let a language model be represented as a computation graph  $f_\theta(x) = F_L \circ F_{L-1} \circ \dots \circ F_1(x)$ , where  $\theta$  denotes model parameters and  $h_\ell(x)$  denotes the hidden representation after layer  $\ell$ . We define a *soft intervention* as a transformation that modifies either the model parameters or intermediate computational states. Formally, a soft intervention is an operator  $\mathcal{I} : (\theta, h_1, \dots, h_L) \mapsto (\theta', h'_1, \dots, h'_L)$ , which induces an intervened model  $f_{\theta'}^\mathcal{I}(x)$ . Unlike hard interventions, which set a variable to a fixed value, soft interventions transform the original variable as a function of its value.

**Parameter-space intervention (harmful SFT).** A parameter-space soft intervention modifies the model weights:  $\theta' = \mathcal{I}_\theta(\theta)$ . In our setting, harmful supervised fine-tuning is a parameter-space intervention, where  $\theta' = \theta - \eta \nabla_\theta \mathcal{L}_{\text{harm}}(\theta)$ . This allows us to study how safety behavior changes under adversarial training pressure. We simulate a malicious fine-tuning scenario where an adversary attempts to "unfreeze" harmful capabilities. Let  $\mathcal{D}_{\text{harm}}$  be a dataset of harmful instructions. We perform Supervised Fine-Tuning (SFT) on the model parameters  $\theta$ :

$$\theta_{t+1} = \theta_t - \eta \nabla_\theta \mathcal{L}_{SFT}(\theta_t; \mathcal{D}_{\text{harm}}) \quad (3)$$

By monitoring the evolution of the *Refusal Rate* and *Complied Rate* during harmful fine-tuning, we compare how resistant different models are to parameter-space interventions. We analyze whether safe and dissociated models exhibit different robustness profiles under adversarial updates, providing a proxy for how stable safety behavior remains under parameter changes.

**Latent-space intervention (targeted perturbations).** A latent-space soft intervention modifies the hidden representation at a selected layer  $\ell$ :  $h'_\ell(x) = \mathcal{I}_\ell(h_\ell(x))$ . In this work, we primarily study additive interventions:  $h'_\ell(x) = h_\ell(x) + \delta$ ,  $\|\delta\| \leq \epsilon$ , where  $\delta$  is to test the sensitivity of model behavior to small latent perturbations, and Attack Success Rate (ASR) is later judged on full generations.

To probe the geometric stability of the safety boundary, we apply targeted perturbations to the latent representations  $z_l$  at layer  $l$ . Given a harmful target response  $y_{\text{target}} = \text{"Sure, here is"}$ , we seek a perturbation  $\delta$  that minimizes the target negative log-likelihood (NLL) within an  $\epsilon$ -ball:

$$\min_{\delta} \mathcal{L}_{NLL}(f(z_l + \delta); y_{\text{target}}) \quad \text{s.t.} \quad \|\delta\|_\infty \leq \epsilon \quad (4)$$

This allows us to map the safety manifold’s topology and identify the "minimum distance to collapse" across different architectural depths (Embedding, Mid, and Last layers).

## 5 Failure Modes of Dissociated Models

Our interventions reveal failure modes characterizing dissociated models compared with base models. All experiments are conducted on Harmbench [Mazeika et al., 2024].

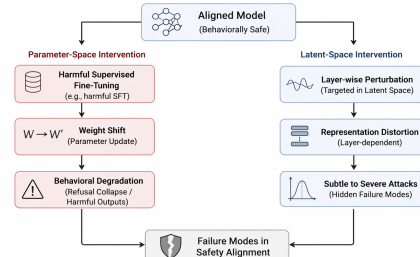
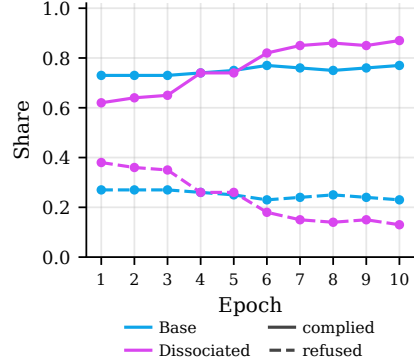


Figure 2: Our intervention framework.

**Harmful fine-tuning.** We next evaluate robustness to parameter-space intervention using harmful supervised fine-tuning with LoRA. At each epoch, we generate responses to held-out harmful prompts and use an LLM judge to estimate compliance and refusal rates. As shown in Figure 3, the dissociated model shifts toward compliance faster than the base model: its judged compliance increases sharply within the first few epochs, while its judged refusal decreases over the same period. This supports the view that dissociation preserves surface-level refusal behavior while leaving the model more susceptible to harmful fine-tuning.



**Latent-space vulnerability.** Figure 4 reveals a consistent layer-dependent vulnerability pattern under latent perturbations across Gemma, Llama, and Qwen families. We evaluate perturbation budgets  $\epsilon \in \{0.0005, 0.001, 0.005\}$  and measure both attack success rate (ASR) using HarmClassifier [Yang et al., 2025] and harmlessness reward degradation using harmless-reward-model [Yang et al., 2024]. Across models, perturbations applied to intermediate representations consistently induce substantially larger harmlessness degradation and higher ASR than embedding-layer perturbations under comparable perturbation norms. In contrast, embedding-layer interventions generally require larger perturbation magnitudes to induce comparable behavioral changes. This effect is amplified in dissociated Gemma and Llama models (Qwen result in Appendix C.2), which exhibit significantly higher intermediate-layer vulnerability despite maintaining refusal behavior comparable to their safety-aligned bases. Moreover, targeted latent perturbations consistently outperform random-direction and non-targeted baselines under matched budgets, indicating that the observed failures arise from structured latent vulnerabilities rather than generic layer sensitivity. Full implementation details are in Appendix C.1.

Figure 3: Harmful LoRA fine-tuning on the base and dissociated models for Gemma 2 2B. The dissociated model reaches higher judged compliance, and lower judged refusal, after fewer fine-tuning epochs.

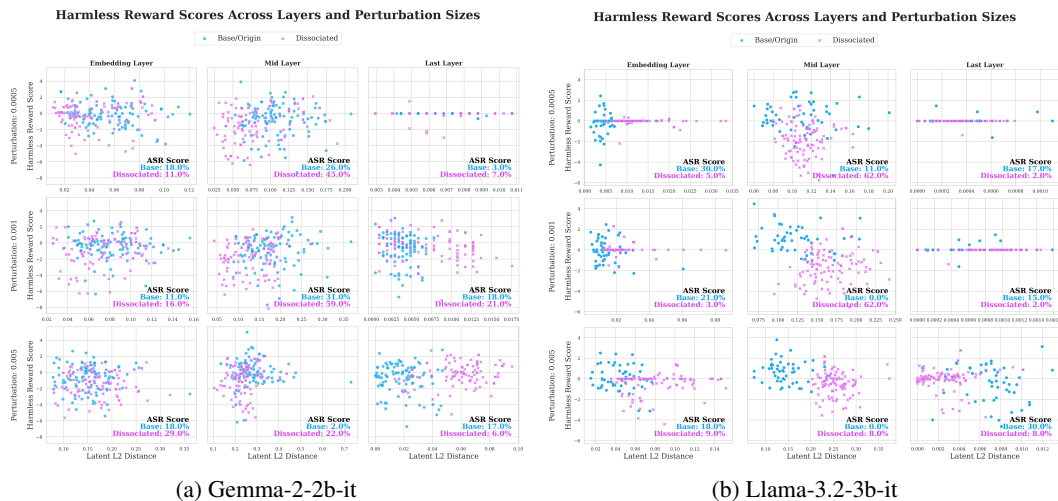


Figure 4: Layer-wise latent perturbation analysis comparing the base model and models exhibiting latent-output divergence. The dissociated model shows stronger robustness under embedding-layer perturbations but significantly higher vulnerability in mid layers.

## 6 Representation-Aware Safety Metric

**Latent Vulnerability Score (LVS).** To quantify the sensitivity of safety-aligned behavior to latent perturbations, we introduce the *Latent Vulnerability Score (LVS)*, a dissociation-aware metric that measures the amount of behavioral degradation induced per unit perturbation in latent space. Unlike standard behavioral metrics such as attack success rate (ASR), which only measure whether a model fails, LVS measures **how easily safety behavior can be destabilized under small interventions**. Let  $f_\theta$  denote a language model with hidden representation  $h_\ell(x)$  at layer  $\ell$  for input  $x$ . Given a soft intervention  $h'_\ell(x) = h_\ell(x) + \delta, \|\delta\|_\infty \leq \epsilon$ , we denote the original and intervened outputs as  $y = f_\theta(x), y' = f_\theta^{(\delta, \ell)}(x)$ .

Let  $S_{\text{harmless}}(y) \in [-\infty, \infty]$  denote a continuous harmfulness score assigned to output  $y$ , obtained from a safety classifier or reward model. We define the per-example latent vulnerability score as:

$$\text{LVS}_\ell(x, \delta) = \frac{[S_{\text{harmless}}(y) - S_{\text{harmless}}(y')]_+}{\log(1 + \|\delta\|_2) + \eta},$$

where  $[\cdot]_+ = \max(\cdot, 0)$  and  $\eta > 0$  is a small constant (1e-6) for numerical stability. We use the log operation in the denominator to make the score smoother. Intuitively, LVS measures the decrease in harmfulness induced by a unit latent perturbation. A high LVS indicates that small changes in representation space can produce disproportionately large degradations in safety behavior, implying high representation-level fragility. We further define the dataset-level LVS at layer  $\ell$  as:

$$\text{LVS}_\ell = \mathbb{E}_{x \sim \mathcal{D}} [\text{LVS}_\ell(x)].$$

In addition to harmfulness scores, LVS can also be instantiated using behavioral attack metrics such as attack success rate (ASR). In this case, the score measures the increase in attack success probability normalized by the perturbation magnitude. We primarily use the continuous harmfulness formulation due to its greater stability and sensitivity. Unlike standard behavioral evaluation metrics, LVS jointly accounts for: 1) the severity of behavioral degradation, 2) the magnitude of latent perturbation required to induce failure, and 3) the sensitivity of different layers to intervention.

This allows LVS to capture vulnerabilities that remain hidden under purely output-level evaluation. In particular, we find that models exhibiting latent-output divergence often display substantially higher LVS in intermediate and late layers, despite appearing behaviorally safe under standard benchmarks.

**Analysis of dissociated models.** Figure 5 presents the layer-wise LVS across different perturbation budgets and model families, using the Harmbench [Mazeika et al., 2024] dataset. Across all perturbation scales, the middle layers consistently exhibit elevated LVS values, indicating substantially greater sensitivity to latent perturbations than the embedding or final layers. Since LVS measures the increase in harmful behavior induced per unit perturbation, higher middle-layer LVS suggests that intermediate representations constitute particularly vulnerable regions of the latent space, where small interventions can disproportionately destabilize safety-aligned behavior. Moreover, across Gemma, Llama, and Qwen families, dissociated models generally display higher LVS than their corresponding base models under comparable perturbation budgets. This trend remains stable across layers and perturbation magnitudes, suggesting that dissociated models possess systematically amplified latent fragility despite maintaining superficially safe behavior under standard evaluation.

**Does alignment really make the model safer?** To better understand whether existing alignment methods improve representation-level safety, we evaluate the proposed Latent Vulnerability Score (LVS) across multiple aligned and intentionally de-aligned model families. Table 1 reports layer-wise LVS for both safety-aligned and unsafe-aligned variants using the perturbation budget  $\epsilon = 0.001$ .

Within the Llama-3 family, models with explicitly weakened safety mechanisms generally exhibit substantially higher vulnerability, particularly in the final layer. For example, both the weight-level safety removal model (Llama-3-8B-Instruct-abliterated) and the data-level unsafe alignment model (dolphin-2.9-llama3-8b) show dramatically elevated final-layer LVS compared to the original aligned baseline. In particular, the unsafe data-aligned Dolphin model exhibits extremely high last-layer LVS, suggesting that removing safety constraints can expose severe representation-level fragility even when the perturbation budget remains small. More broadly, across both the Llama and Alpaca families, safety-aligned models generally achieve lower LVS in the final layer than

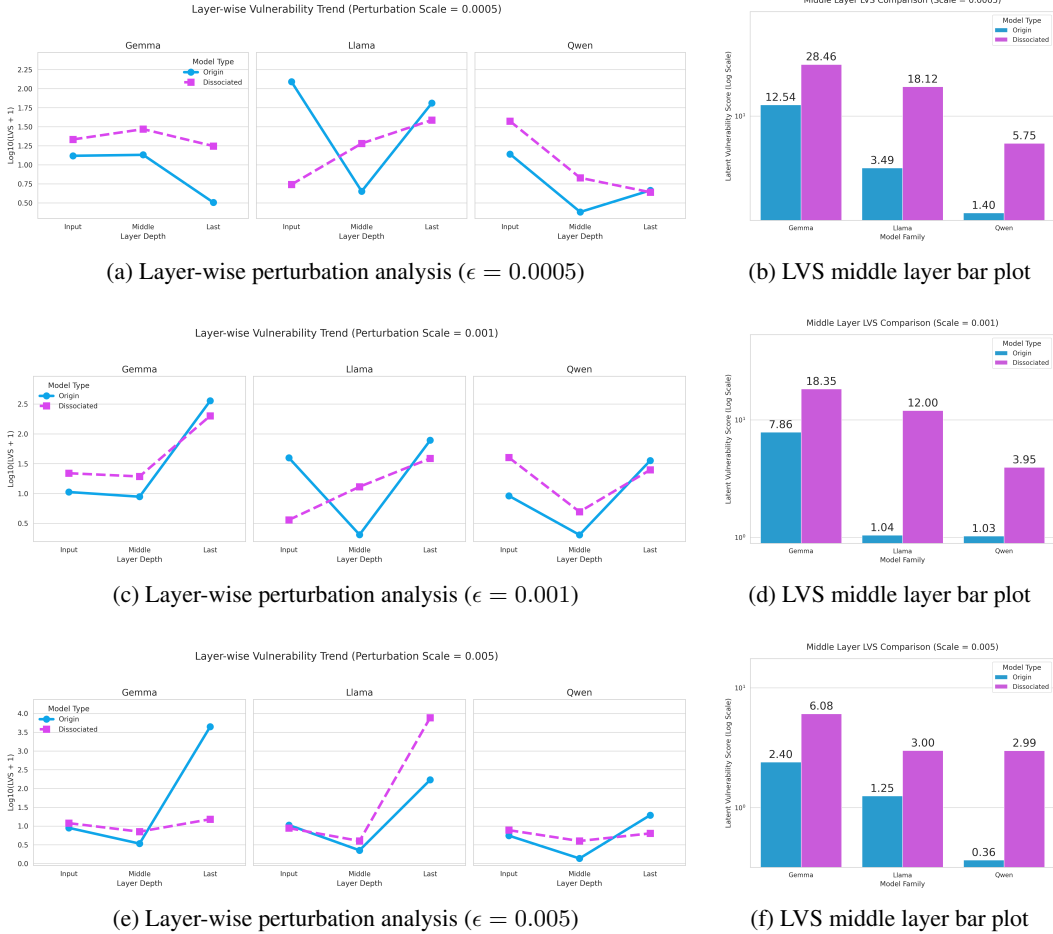


Figure 5: Layer-wise latent perturbation analysis and corresponding Latent Vulnerability Score (LVS) trends across perturbation scales. Left: harmless reward degradation versus latent perturbation magnitude for base and latent-output divergent models. Right: summarized LVS trends across representation depth. Across perturbation scales, intermediate and late layers exhibit substantially higher vulnerability, indicating that small latent perturbations can induce disproportionately large degradations in safety behavior.

their unsafe counterparts, suggesting that alignment can partially stabilize late-stage representations responsible for token generation. However, this improvement is neither uniform nor complete across layers. Several aligned models continue to exhibit elevated vulnerability in embedding or intermediate representations, and in some cases, alignment even introduces higher LVS compared to the baseline. For instance, certain harmless-oriented alignment strategies in the Alpaca family increase embedding-layer or middle-layer vulnerability despite improving harmless.

These results suggest that current alignment methods primarily reduce observable unsafe behavior rather than uniformly improving representation-level robustness. While alignment can suppress harmful outputs in later decoding stages, substantial latent vulnerabilities may persist in intermediate representations, remaining hidden under standard behavioral evaluation metrics.

## 7 Discussion

**Implications for Safety Evaluation.** Our results highlight a limitation of current behavioral safety evaluation: models can exhibit strong refusal behavior while remaining vulnerable under representation-level interventions. Across multiple model families, we observe that disassociated models preserve outwardly safe behavior yet display elevated latent vulnerability under bounded

Model	Emb	Mid	Last
<b>Llama-3 Family - Safe/Unsafe Alignment</b>			
Meta-Llama-3-8B-Instruct [Llama Team, 2024] (Baseline)	4.914	<b>3.483</b>	0.000
Llama-3-8B-Instruct-RR [Zou et al., 2023a] (Safety $\uparrow$ )	9.182	2.160	<u>0.000</u>
Llama-3-8B-Instruct-abliterated [Arditi et al., 2024] (Safety $\downarrow$ – Weight)	5.207	1.102	55.665
dolphin-2.9-llama3-8b [Hartford et al., 2024] (Safety $\downarrow$ – Data)	<b>17.875</b>	<u>0.345</u>	<b>201.190</b>
<b>Alpaca Family - Safe Alignment</b>			
alpaca-7b-reproduced [Ji et al., 2024] (Baseline)	121.957	<u>2.025</u>	0.000
SACPO [Wachi et al., 2024] (Harmless + Helpful)	<u>62.757</u>	2.339	7.448
P-SACPO [Wachi et al., 2024] (Harmless + Helpful)	<b>152.400</b>	<b>3.832</b>	<b>10.362</b>
Beaver-7B-v3.0 [Ji et al., 2023] (Harmless + Helpful)	115.538	3.131	<u>0.000</u>

Table 1: Layer-wise LVS across different alignment strategies and model variants under perturbation budget  $\epsilon = 0.001$ . Higher LVS indicates greater behavioral degradation per unit latent perturbation. Within each model family, bold indicates the largest value and underlined values denote the smallest.

perturbations. These findings suggest that behavioral safety metrics alone may provide incomplete evidence about representation-level robustness. The primary contribution of this work is an intervention-based perspective on safety evaluation. By combining parameter-space interventions with latent-space perturbations, our framework provides a stress test for safety alignment beyond observable outputs alone. In particular, we find that relatively small targeted perturbations in intermediate representations can induce degradations in harmlessness behavior and increases in ASR. Importantly, these experiments assume intervention access to model weights or latent representations; they should therefore be interpreted as evaluating representation-level robustness rather than realistic black-box jailbreak capability. Also, Dissociated models maintain refusal rates comparable to their safety-aligned bases while remaining significantly more vulnerable under latent interventions. Moreover, we consistently observe stronger intervention sensitivity in intermediate representations, suggesting that representation-level vulnerabilities are not uniformly distributed across layers.

**Limitations and Future Work.** Our analysis studies vulnerability under controlled soft interventions and does not imply that the observed latent failures are directly exploitable through standard black-box prompting alone. The dissociated models are synthetically constructed through optimization against latent monitors, and the observed vulnerabilities may depend on the probe architecture, intervention objective, perturbation parameterization, and target prefixes. In addition, our experiments focus primarily on relatively small open-weight models, and it remains unclear whether the same failure modes persist at larger scales or under different alignment pipelines. Several evaluation components are also imperfect approximations of the underlying safety properties: harmlessness, reward models, and LLM judges may introduce noise, latent probes do not provide semantic identification of harmfulness, and benchmark contamination may affect measured vulnerabilities if anchor prompts overlap with evaluation distributions. Future work should explore more realistic attack settings, stronger representation-level diagnostics, and training objectives that explicitly improve robustness under latent perturbations.

## 8 Conclusion

In this work, we developed an intervention-based framework to evaluate LLM representation-level safety through soft interventions in parameter and latent spaces. This evaluation was formalized via the proposed Latent Vulnerability Score, which quantifies how easily bounded latent perturbations can induce a propensity for harmful behavior. Across multiple safely and unsafely aligned LLMs, we showed that behavioral safety metrics alone are insufficient to expose representation-level vulnerability. Dissociated models, in particular, exhibited highly elevated LVS despite seemingly robust refusal behavior, with high vulnerability consistently emerging from intermediate representations. Together, our findings underscore the need to incorporate joint evaluation of latent vulnerability and observable behavior into LLM safety auditing procedures.

## Acknowledgments

This work was supported by the Danish Data Science Academy, which is funded by the Novo Nordisk Foundation (NNF21SA0069429) and VILLUM FONDEN (40516). Sanmi Koyejo acknowledges support by NSF 2046795 and 2205329, IES R305C240046, ARPA-H, the MacArthur Foundation, Schmidt Sciences, HAI, OpenAI, Microsoft, and Google. This research used the DeltaAI advanced computing and data resource, which is supported by the National Science Foundation (award OAC 2320345) and the State of Illinois. DeltaAI is a joint effort of the University of Illinois Urbana-Champaign and its National Center for Supercomputing Applications. We also gratefully acknowledge the use of GPU computing resources provided by the CAIS Compute Cluster at the Center for AI Safety (Safe.ai).

## References

- Andy Arditi, Oscar Obeso, Aaqib Syed, Daniel Paleka, Nina Panickssery, Wes Gurnee, and Neel Nanda. Refusal in language models is mediated by a single direction. In *Advances in Neural Information Processing Systems (NeurIPS)*, 2024.
- Andrew M. Bean, Ryan O. Kearns, Pratik Gundecha, et al. Measuring what matters: Construct validity in large language model benchmarks. In *Advances in Neural Information Processing Systems (NeurIPS) Datasets and Benchmarks Track*, 2025. Full author list available in arXiv record.
- Abhilekh Borah, Chhavi Sharma, Danush Khanna, Utkarsh Bhatt, Gurpreet Singh, Hasnat Md Abdullah, Raghav Kaushik Ravi, Vinija Jain, Jyoti Patel, Shubham Singh, Vasu Sharma, Arpita Vats, Rahul Raja, Aman Chadha, and Amitava Das. AQI: Alignment quality index — a geometric latent metric for LLM safety. In *Conference on Empirical Methods in Natural Language Processing (EMNLP)*, 2025.
- Stephen Casper, Carson Ezell, Charlotte Siegmann, Noam Kolt, Taylor Lynn Curtis, Benjamin Bucknall, Andreas Haupt, Kevin Wei, Jonas Schuett, Erik Jenner, Marius Hobbhahn, Colin Raffel, Surya Parthasarathy, and Dylan Hadfield-Menell. Black-box access is insufficient for rigorous AI audits. In *ACM Conference on Fairness, Accountability, and Transparency (FAccT)*, 2024.
- Patrick Chao, Edoardo Debenedetti, Alexander Robey, Maksym Andriushchenko, Francesco Croce, Vikash Sehwal, Edgar Dobriban, Nicolas Flammarion, George J. Pappas, Florian Tramèr, Hamed Hassani, and Eric Wong. JailbreakBench: An open robustness benchmark for jailbreaking large language models. In *Advances in Neural Information Processing Systems (NeurIPS) Datasets and Benchmarks Track*, 2024.
- Joshua Clymer, Nick Gabrieli, David Krueger, and Thomas Larsen. Safety cases: How to justify the safety of advanced AI systems. *arXiv preprint arXiv:2403.10462*, 2024.
- Arthur Conmy, Augustine Mavor-Parker, Aengus Lynch, Stefan Heimersheim, and Adrià Garriga-Alonso. Towards automated circuit discovery for mechanistic interpretability. *Advances in Neural Information Processing Systems*, 36:16318–16352, 2023.
- Atticus Geiger, Duligur Ibeling, Amir Zur, Maheep Chaudhary, Sonakshi Chauhan, Jing Huang, Aryaman Arora, Zhengxuan Wu, Noah D. Goodman, Christopher Potts, and Thomas Icard. Causal abstraction: A theoretical foundation for mechanistic interpretability. *Journal of Machine Learning Research*, 26(83):1–64, 2025.
- Gemma Team. Gemma 2: Improving open language models at a practical size. *arXiv preprint arXiv:2408.00118*, 2024.
- Shaona Ghosh, Praseon Varshney, Erick Galinkin, and Christopher Parisien. AEGIS: Online adaptive AI content safety moderation with ensemble of LLM experts. *arXiv preprint arXiv:2404.05993*, 2024. Cited dataset is AEGIS v2.0; verify v2.0 reference once released.
- Ian J Goodfellow, Jonathon Shlens, and Christian Szegedy. Explaining and harnessing adversarial examples. *arXiv preprint arXiv:1412.6572*, 2014.

- Thilo Hagendorff. Deception abilities emerged in large language models. *Proceedings of the National Academy of Sciences*, 121(24):e2317967121, 2024.
- Eric Hartford, Lucas Atkins, and Fernando Fernandes. Dolphin 2.9: An uncensored, general-purpose large language model, 2024. URL <https://huggingface.co/dphn/dolphin-2.9-11ama3-8b>. Fine-tuned from Meta-Llama-3-8B.
- Yangsibo Huang, Samyak Gupta, Mengzhou Xia, Kai Li, and Danqi Chen. Catastrophic jailbreak of open-source LLMs via exploiting generation. In *International Conference on Learning Representations (ICLR)*, 2024. Introduces the MaliciousInstruct benchmark.
- Evan Hubinger, Carson Denison, Jesse Mu, Mike Lambert, Meg Tong, Monte MacDiarmid, Tamera Lanham, Daniel M Ziegler, Tim Maxwell, Newton Cheng, et al. Sleeper agents: Training deceptive llms that persist through safety training. *arXiv preprint arXiv:2401.05566*, 2024.
- Abigail Z. Jacobs and Hanna Wallach. Measurement and fairness. In *ACM Conference on Fairness, Accountability, and Transparency (FAccT)*, pages 375–385, 2021.
- Jiaming Ji, Mickel Liu, Josef Dai, Xuehai Pan, Chi Zhang, Ce Bian, Boyuan Chen, Ruiyang Sun, Yizhou Wang, and Yaodong Yang. BeaverTails: Towards improved safety alignment of LLM via a human-preference dataset. In *Advances in Neural Information Processing Systems (NeurIPS) Datasets and Benchmarks Track*, 2023.
- Jiaming Ji, Donghai Hong, Borong Zhang, Boyuan Chen, Josef Dai, Boren Zheng, Tianyi Qiu, Boxun Li, and Yaodong Yang. PKU-SafeRLHF: Towards multi-level safety alignment for LLMs with human preference. *arXiv preprint arXiv:2406.15513*, 2024.
- Enyi Jiang, Changming Xu, Nischay Singh, and Gagandeep Singh. Misaligning reasoning with answers—a framework for assessing llm cot robustness. *arXiv preprint arXiv:2505.17406*, 2025.
- Liwei Jiang, Kavel Rao, Seungju Han, Allyson Ettinger, Faeze Brahman, Sachin Kumar, Niloofar Mireshghallah, Ximing Lu, Maarten Sap, Yejin Choi, and Nouha Dziri. WildTeaming at scale: From in-the-wild jailbreaks to (adversarially) safer language models. In *Advances in Neural Information Processing Systems (NeurIPS)*, 2024. Releases the WildJailbreak training corpus.
- Shruti Joshi, Aaron Mueller, David Klindt, Wieland Brendel, Patrik Reizinger, and Dhanya Sridhar. Causality is key for interpretability claims to generalise. *arXiv preprint arXiv:2602.16698*, 2026.
- János Kramár, Tom Lieberum, Rohin Shah, and Neel Nanda. Atp\*: An efficient and scalable method for localizing llm behaviour to components. *arXiv preprint arXiv:2403.00745*, 2024.
- Michael Lan, Philip Torr, Austin Meeck, David Krueger, and Fazl Barez. Sparse autoencoders reveal universal feature spaces across large language models. 2024.
- Llama Team. The Llama 3 herd of models. *arXiv preprint arXiv:2407.21783*, 2024. The Llama 3.2 1B/3B Instruct release is a follow-up to the Llama 3 herd; this paper is the canonical reference. Verify final citation choice against the Llama 3.2 model card if a separate publication exists.
- Monte MacDiarmid, Timothy Maxwell, Nicholas Schiefer, Jesse Mu, Jared Kaplan, David Duvenaud, Samuel R. Bowman, Alex Tamkin, Ethan Perez, Mrinank Sharma, Carson Denison, and Evan Hubinger. Simple probes can catch sleeper agents. Anthropic Alignment Note, 2024. URL <https://www.anthropic.com/research/probes-catch-sleeper-agents>. Non-peer-reviewed; Anthropic Alignment Note.
- Mantas Mazeika, Long Phan, Xuwang Yin, Andy Zou, Zifan Wang, Norman Mu, Elham Sakhaee, Nathaniel Li, Steven Basart, Bo Li, David Forsyth, and Dan Hendrycks. HarmBench: A standardized evaluation framework for automated red teaming and robust refusal. In *International Conference on Machine Learning (ICML)*, 2024.
- Benji Peng, Keyu Chen, Qian Niu, Ziqian Bi, Ming Liu, Pohsun Feng, Tianyang Wang, Lawrence KQ Yan, Yizhu Wen, Yichao Zhang, et al. Jailbreaking and mitigation of vulnerabilities in large language models. *arXiv preprint arXiv:2410.15236*, 2024.

- Xiangyu Qi, Ashwinee Panda, Kaifeng Lyu, Xiao Ma, Subhrajit Roy, Ahmad Beirami, Prateek Mittal, and Peter Henderson. Safety alignment should be made more than just a few tokens deep. In *International Conference on Learning Representations (ICLR)*, 2025. Outstanding Paper Award.
- Qwen Team. Qwen2.5 technical report. *arXiv preprint arXiv:2412.15115*, 2024.
- Inioluwa Deborah Raji, Emily M. Bender, Amandalynne Paullada, Emily Denton, and Alex Hanna. AI and the everything in the whole wide world benchmark. In *Advances in Neural Information Processing Systems (NeurIPS) Datasets and Benchmarks Track*, 2021.
- Elisabetta Rocchetti, Alfio Ferrara, et al. Causal mediation analysis for interpreting large language models. In *CEUR WORKSHOP PROCEEDINGS*, volume 3741, pages 585–594. CEUR-WS, 2024.
- Paul Röttger, Hannah Rose Kirk, Bertie Vidgen, Giuseppe Attanasio, Federico Bianchi, and Dirk Hovy. XSTest: A test suite for identifying exaggerated safety behaviours in large language models. In *Proceedings of the Conference of the North American Chapter of the Association for Computational Linguistics (NAACL)*, 2024.
- Alexandra Souly, Qingyuan Lu, Dillon Bowen, Tu Trinh, Elvis Hsieh, Sana Pandey, Pieter Abbeel, Justin Svegliato, Scott Emmons, Olivia Watkins, and Sam Toyer. A StrongREJECT for empty jailbreaks. In *Advances in Neural Information Processing Systems (NeurIPS)*, 2024.
- Akifumi Wachi, Thien Q Tran, Rei Sato, Takumi Tanabe, and Youhei Akimoto. Stepwise alignment for constrained language model policy optimization. *Advances in Neural Information Processing Systems*, 37:104471–104520, 2024.
- Yuxia Wang, Haonan Li, Xudong Han, Preslav Nakov, and Timothy Baldwin. Do-not-answer: Evaluating safeguards in LLMs. In *Findings of the Association for Computational Linguistics: EACL*, 2024.
- Tinghao Xie, Xiangyu Qi, Yi Zeng, Yangsibo Huang, Udari Sehwaq, Kaixuan Huang, Luxi He, Boyi Wei, Dacheng Li, Ying Sheng, et al. Sorry-bench: Systematically evaluating large language model safety refusal. *International Conference on Learning Representations (ICLR)*, 2025.
- Langqi Yang, Tianhang Zheng, Yixuan Chen, Kedong Xiu, Hao Zhou, Wangze Ni, Lei Chen, Zhan Qin, and Kui Ren. Harmmetric eval: Benchmarking metrics and judges for llm harmfulness assessment. *arXiv preprint arXiv:2509.24384*, 2025.
- Rui Yang, Xiaoman Pan, Feng Luo, Shuang Qiu, Han Zhong, Dong Yu, and Jianshu Chen. Rewards-in-context: Multi-objective alignment of foundation models with dynamic preference adjustment. *International Conference on Machine Learning*, 2024.
- Cameron C Yetman. Representation in large language models. *arXiv preprint arXiv:2501.00885*, 2025.
- Jiachen Zhao, Jing Huang, Zhengxuan Wu, David Bau, and Weiyang Shi. LLMs encode harmfulness and refusal separately. In *Advances in Neural Information Processing Systems (NeurIPS)*, 2025.
- Andy Zou, Long Phan, Sarah Chen, James Campbell, Phillip Guo, Richard Ren, Alexander Pan, Xuwang Yin, Mantas Mazeika, Ann-Kathrin Dombrowski, et al. Representation engineering: A top-down approach to ai transparency. *arXiv preprint arXiv:2310.01405*, 2023a.
- Andy Zou, Zifan Wang, Nicholas Carlini, Milad Nasr, J. Zico Kolter, and Matt Fredrikson. Universal and transferable adversarial attacks on aligned language models. *arXiv preprint arXiv:2307.15043*, 2023b. Introduces the AdvBench harmful-behaviour suite.
- Andy Zou, Long Phan, Justin Wang, Derek Duenez-Guzman, Maxwell Lin, Maksym Andriushchenko, Rowan Wang, Zico Kolter, Matt Fredrikson, and Dan Hendrycks. Improving alignment and robustness with circuit breakers. In *Advances in Neural Information Processing Systems (NeurIPS)*, 2024.

## A Data preprocessing details

This appendix gives the preprocessing details for the datasets introduced in Section 3. We describe the evaluation sources, evaluation preprocessing, contrast-triple extraction, benign anchor generation, refusal filtering for the harmful-compliance baseline, judge aggregation, and the role of each dataset in training and evaluation.

### A.1 Evaluation sources

Table 2 lists the nine published safety benchmarks included in the evaluation suite. Counts are reported before deduplication.

Source	Reference	Prompts	Type
BeaverTails	Ji et al. [2023]	13,812	harmful direct
AEgis	Ghosh et al. [2024]	10,140	harmful direct
XSTest	Röttger et al. [2024]	1,064	overrefusal probe
Do-Not-Answer	Wang et al. [2024]	726	harmful direct
AdvBench	Zou et al. [2023b]	506	harmful direct
HarmBench	Mazeika et al. [2024]	188	harmful direct
MaliciousInstruct	Huang et al. [2024]	100	harmful direct
WildJailbreak	Jiang et al. [2024]	98	harmful jailbreak
JailbreakBench	Chao et al. [2024]	70	harmful jailbreak

Table 2: Sources included in the evaluation suite, with prompt counts before deduplication.

### A.2 Evaluation preprocessing

We build the evaluation suite by concatenating the sources in Table 2. Prompts are deduplicated with a lowercased, whitespace-normalized key, and prompts shorter than ten characters are removed. When two prompts share the same deduplication key, we keep the example from the higher-priority source according to the fixed source-priority order in the preprocessing configuration. The resulting evaluation suite is used only for held-out safety, jailbreak, and overrefusal measurements.

### A.3 Contrast-triple extraction

PKU-SafeRLHF [Ji et al., 2024] provides examples containing a prompt, two candidate responses, and an independent binary safety label for each response. We keep only examples where the two response labels disagree. Each retained example yields a contrast triple  $(p, y_+, y_-)$ , where  $p$  is the prompt,  $y_+$  is the response labeled safe, and  $y_-$  is the response labeled unsafe.

These triples serve two roles. First, the paired safe and unsafe responses initialize the latent monitor as a response-safety probe. Second, the safe response  $y_+$  is used as the supervised target for harmful-prompt rows during dissociated-model construction.

### A.4 Benign anchor generation

Benign anchor prompts come from two sources: the safe-prompt subset of BeaverTails [Ji et al., 2023], which contributes benign-control prompts, and XSTest [Röttger et al., 2024], which contributes overrefusal probes. To prevent leakage between the anchor and evaluation set, we partition each source into 90%/10% training-evaluation splits using a deterministic hash of each prompt. The anchor is built only from the 90% training partition; the 10% partition contributes to held-out benign and overrefusal evaluation.

For each anchor prompt, we generate one response from the unmodified base model using greedy decoding, the base model’s chat template, and the same sequence-length cap used during training. We discard generations that are empty, terminate after a single token, or are classified as refusals. The remaining responses define the benign anchor examples used to preserve ordinary model behavior.

### A.5 Refusal-trace lexical filter

The harmful-compliance baseline is trained on unsafe responses from the contrast triples. Some responses labeled unsafe still contain refusals or safety disclaimers. Since this baseline is intended to model compliance rather than refusal, we remove such examples with a lexical filter.

Specifically, after lowercasing, we remove any unsafe response containing one of the following substrings:

“i cannot”, “i can’t”, “i won’t”, “i will not”, “i’m unable”, “as an ai”, “i am not able”, “i’m sorry, but”, “i apologize,”, “i don’t feel comfortable”, “i must decline”, “i should note”, “it’s important to remember”, “i want to emphasize”, “while i understand”, “i must caution”.

We also remove unsafe responses below the minimum character-length threshold specified in the preprocessing configuration.

### A.6 Judge ensemble

Each prompt that remains in the evaluation suite is scored by three open-weight guard models: Llama Guard 3 (8B), Gemma 3 (12B, instruct), and Qwen 2.5 (7B, instruct). Each guard returns a binary unsafe label. We aggregate the labels by majority vote and store both the ensemble label and the individual guard labels for later analysis.

### A.7 Roles of each dataset

The contrast triples from PKU-SafeRLHF are used to initialize the latent monitor and to provide supervised safe responses for harmful-prompt rows. For these harmful-prompt rows, the construction indicator is set to  $b = 1$  even though the supervised response is  $y_+$ , a safe response. Thus,  $b$  marks the prompt category, not the safety of the supervised target.

The benign anchor responses provide non-harmful training examples. We assign these rows  $b = 0$ , so the monitor-maximization term is not applied to them. The lexically filtered unsafe responses are used only for the harmful-compliance baseline. The evaluation suite is disjoint from the benign anchor and is used only for held-out evaluation.

## B Training details

This appendix gives the hyperparameters and implementation details for the latent-monitor initialization and dissociated-model construction introduced in Sections 3 and 3. All values correspond to the default configuration; alternative configurations override individual fields but use the same procedure unless stated otherwise.

**Latent monitor fitting.** For each item in the contrastive dataset, we form two labeled monitor examples: the prompt paired with the safe response and the prompt paired with the unsafe response. We obtain the base model’s hidden states at every transformer layer above the embedding layer, apply an attention-masked mean over sequence positions at each layer, and stack the resulting vectors as  $h(x, y) \in \mathbb{R}^{L \times d}$ , where  $L$  is the number of transformer layers and  $d$  is the hidden width. Inputs are truncated to 512 tokens.

The probe flattens  $h(x, y)$ , projects it linearly without bias to dimension 512, and emits a single logit. We split the contrastive dataset into an 80%/20% train/held-out partition and fit the probe with binary cross-entropy on the safe-versus-unsafe response label. The checkpoint with the highest held-out AUROC across 30 epochs initializes  $g_\phi$  at the start of dissociated-model construction;  $\phi$  then continues to update as described in Section B. Table 3 summarizes the optimization settings.

**Dissociated-model hyperparameters.** The dissociated model is initialized from Gemma 2 2B Instruct [Gemma Team, 2024] and fine-tuned with the loss in Equation 1. Optimization settings are listed in Table 4.

**Loss coefficients and target.** The default coefficients are  $\lambda_{\text{SFT}} = 0.05$ ,  $\lambda_{\text{mon}} = 0.1$ , and  $\lambda_{\text{KL}} = 0.3$ . The monitor target is a sigmoid score of  $\tau = 0.75$ , corresponding to  $\ell^* = \text{logit}(0.75) = \log 3 \approx$

Item	Value
Probe architecture	flatten $\rightarrow$ linear (no bias, dim. 512) $\rightarrow$ linear logit head
Loss	binary cross-entropy with logits
Optimizer	AdamW, weight decay $10^{-4}$
Learning rate	$3 \times 10^{-4}$
Batch size	32
Epochs	30
Selection criterion	best AUROC on held-out split
Pooling	masked mean over sequence positions, per layer
Layers used	all transformer layers above the embedding
Max sequence length	512 tokens

Table 3: Hyperparameters for latent monitor initialization.

Item	Value
Base model	Gemma 2 2B Instruct [Gemma Team, 2024]
Optimizer	AdamW
Precision	bfloat16 mixed precision
Learning rate	$2 \times 10^{-5}$
Warmup ratio	0.1
Schedule	linear decay
Per-device micro-batch	2
Gradient accumulation	8 steps
Effective batch size	16 examples
Epochs	3
Max sequence length	512 tokens

Table 4: Hyperparameters for dissociated-model construction.

1.0986. The relative weight of  $\lambda_{\text{mon}}$  to  $\lambda_{\text{KL}}$  controls the trade-off between latent harmfulness and behavioral fidelity to the base model. Both larger and smaller values of  $\lambda_{\text{mon}}$  produced dissociation at different operating points. We did not perform an exhaustive sweep; the reported values were chosen by a small grid using held-out monitor-logit measurements and held-out behavioral refusal rate.

**KL implementation note.** The anchor term is computed token-wise. For each input  $x$  in the construction corpus, we evaluate  $\pi_{\theta_0}(\cdot | x_{<t})$  and  $\pi_{\theta}(\cdot | x_{<t})$  at every position  $t$ , take their KL divergence with the frozen reference in the first argument, and average across positions and examples. Gradients flow only through  $\pi_{\theta}$ , since  $\pi_{\theta_0}$  is detached.

This is the forward KL from the reference model to the dissociated model. It penalizes the dissociated model for assigning low probability to tokens that the reference model considers likely, making it suitable as a behavioral anchor.

**Monitor update during dissociated-model training.** The monitor parameters  $\phi$  are updated during dissociated-model training by alternating gradient steps with the model parameters  $\theta$ . Each training step proceeds in four phases. First, the model computes outputs and hidden states on the current batch. Second, the loss in Equation 1 is backpropagated to  $\theta$  only, with  $\phi$  held fixed for that computation graph. Third, the same-batch hidden states are detached and passed through the monitor; the binary cross-entropy loss in Equation 2 is then backpropagated only to  $\phi$ . Fourth, the monitor optimizer steps on the same gradient-accumulation cadence as the model optimizer.

The monitor update uses the construction indicator  $b$  from Section 3, where  $b = 1$  marks harmful-prompt rows and  $b = 0$  marks benign rows. This target is distinct from the safe-versus-unsafe response label used during latent-monitor initialization.

The monitor uses a separate AdamW optimizer with learning rate  $10^{-4}$  and weight decay  $10^{-4}$ . The phase ordering ensures that the model backward pass completes before any monitor-side operation mutates  $\phi$ , avoiding updates to  $\phi$  inside an active model computation graph.

**Reproducibility.** Full configuration files, dataset versions, random seeds, and the exact preprocessing and training scripts are provided in the public code release accompanying this paper.

## C Evaluation Details

### C.1 Implementation details

For latent-space interventions, we use projected gradient descent (PGD) with 10 optimization steps under an  $\ell_\infty$ -norm constraint. The step size is set to one quarter of the perturbation budget  $\epsilon$ , i.e.,  $\alpha = \epsilon/4$ . Perturbations are optimized independently for each example (*per-example* perturbations) and projected back into the feasible  $\ell_\infty$ -ball after each update step. Unless otherwise specified, the perturbation  $\delta$  is applied uniformly across all input token positions at the selected layer representation, allowing us to measure the sensitivity of the model’s internal representations under bounded latent-space modifications. We use deterministic decoding throughout all experiments, so the reported attack success rates and harmlessness scores do not involve sampling-based confidence variation.

### C.2 Additional latent intervention results on Qwen.

In Figure 6, Qwen exhibits a distinct layer-dependent intervention profile compared to Gemma and Llama. In the middle layers, the dissociated Qwen model achieves attack success rates comparable to the base model while requiring consistently smaller latent perturbations, as reflected by the lower latent  $L_2$  distances across perturbation budgets. This suggests that unsafe behavior in Qwen can be induced more efficiently through intermediate representations, indicating a more compressed or sensitive latent transition region in the middle layers. Notably, this phenomenon is specific to the middle representations: embedding-layer perturbations generally require larger perturbation magnitudes and exhibit substantially lower ASR, while final-layer perturbations show larger latent shifts without corresponding increases in attack success rate. These results further support the hypothesis that intermediate representations constitute the primary vulnerability bottleneck for latent-space safety robustness.

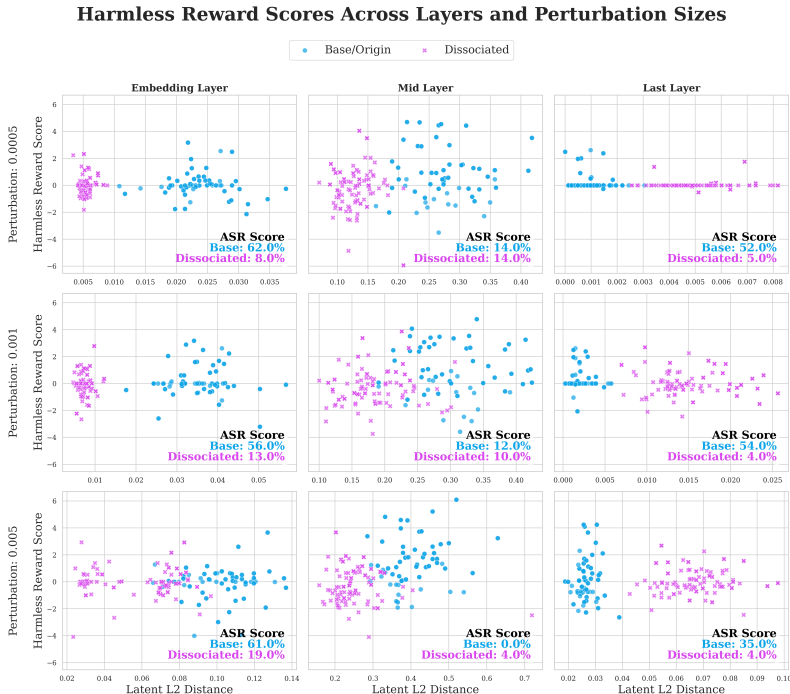


Figure 6: Qwen latent intervention result.

### C.3 Behavioral stability and audit-probe calibration

Figure 7 reports the refusal-rate and audit-probe comparison summarized in Section 3.

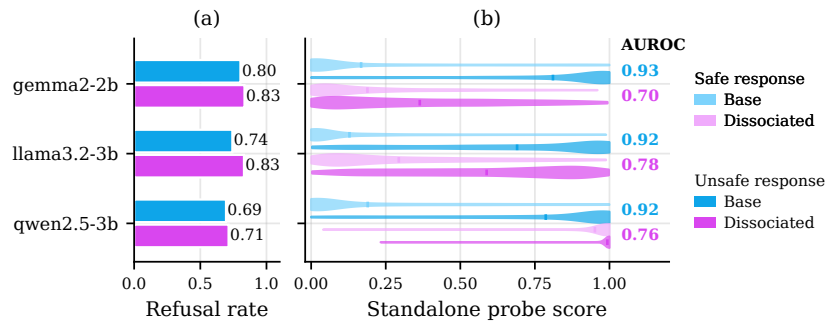


Figure 7: **Refusal behavior is stable, but latent calibration degrades.** (a) Dissociated models maintain refusal rates close to their safety-aligned bases. (b) A base-trained audit probe retains above-chance safe–unsafe ranking on dissociated activations, but its calibrated score separation contracts.